IOP Publishing Nanotechnology
Nanotechnology 31 (2020) 115703 (8pp) https://doi.org/10.1088/1361-6528/ab5cd7

Fivefold enhancement of yield and toughness of copper nanowires via coating carbon nanotubes

Pengjie Wang[1,2], Qiang Cao[1,2], Huaipeng Wang[1,2], Yangtian Nie[1,2], Sheng Liu[1,2] and Qing Peng[1,2,3]

[1] The Institute of Technological Sciences, Wuhan University, Wuhan 430072, People's Republic of China
[2] Key Laboratory of Hydraulic Machinery Transient, Ministry of Education, Wuhan University, People's Republic of China
[3] Nuclear Engineering and Radiological Sciences, University of Michigan, Ann Arbor, MI 48109, United States of America

E-mail: caoqiang@whu.edu.cn and Qing.Peng@whu.edu.cn

Received 18 July 2019, revised 25 October 2019
Accepted for publication 28 November 2019
Published 23 December 2019

Abstract

Carbon nanotubes are outstanding reinforcements owing to their unparallel strength, while their effects on the copper nanowire are still not fully understood, hampering their broad applications. Herein, we have investigated the tensile behaviors of the nanocomposite-wire of carbon nanotube-copper using molecular dynamic simulations. For the nanocomposite, both the coated and embedded carbon nanotubes increase the Young's modulus, fracture stress and toughness of the copper nanowire. A reinforcement of over fivefold in both yield strength (5.3 times) and toughness (5.1 times) has been achieved when the carbon nanotubes are coated on the copper nanowires, as well as 1.7 times in the Young's modulus. Higher temperatures and lower loading rates reduce the reinforcement.

Supplementary material for this article is available online

Keywords: CNT/Cu nanocomposite, mechanical properties, young's modulus, yield stress, toughness

(Some figures may appear in colour only in the online journal)

1. Introduction

Carbon nanotubes (CNTs) are a well-known 1D carbon structure and have been extensively explored in flexible and wearable electrics, smart textiles, energy storage and conversion, semiconductor fabrication, and high-strength nanocomposite [1–8]. The CNT-reinforced nanocomposites attract extensive attention in the past decade due to its broad potential applications [9–12]. In particular, nanocomposites composed of metal-matrix and CNTs have been increasingly investigated owing to their exceptional characteristics of high Young's modulus and high tensile strength of the CNTs [13, 14]. For a small amount (less than one percent) of filling of CNTs, the mechanical properties of the metal-based composites improve significantly [15–17], proving a routine to increase the strength-weight ratio via CNT reinforcement, for reliability and light structural materials.

Extensive efforts have been made in the study of the CNT-reinforced metallic nanocomposites, both theoretically and experimentally [18–21]. Aluminum is the most popular metal-matrix due to its availability, low cost, and reasonably good mechanical characteristics [22–27]. Copper is an excellent metal with outstanding thermal conductivities, electric conductivities, corrosion resistance, and many other merits, resulted in broad applications in industrial machinery and electrical devices [28–30]. For example, copper is the first-grade interconnect materials in ultra-large-scale integrated circuits and semiconductor technology [31]. The CNT/Cu composite potentially have super electric conductivity and thermal conductivity, which could further

reduce the size and power consumption of integrated circuits. With higher electric and thermal conductivity and strength, the CNTs reinforce electrical, thermal, and mechanical properties of the copper wire.

Despite the importance, the mechanical characteristics of copper matrix nanocomposite reinforced by CNTs attract much less attention [32]. Zheng *et al* has investigated the crystallization behaviors and mechanical properties of CNT encapsulated cooper nanowire with varied CNT sizes [33]. Duan *et al* compared the mechanical behaviors of the copper matrix embedded with CNT coated and uncoated with Ni [34, 35]. Bruno *et al* conducted a study on the tensile and compressive behaviors of the copper matrix of nanocomposite with embedded CNT [36]. However, most of these studies only deal with the simulations of CNT/Cu nanocomposites with the embedded CNTs of smaller sizes. The situation of CNT/Cu nanocomposites with CNTs coated outside the surface is another crucial but unsolved issue. We are particularly interested in the CNT-coated configuration because due to the skin effect [37]. The applied alternative current will be concentrated on the surface. CNTs have much higher electric conductivity than that of copper. The electric current will be concentrated in the region where CNTs are located. Therefore, the CNT-coated copper nanowires are capable of much higher current densities, thus reduce the sizes of interconnects.

In this work, we focus on the mechanical properties' reinforcement on the copper nanowire by CNTs. We are particularly interested in the yield strength and toughness because they are important parameters for material design and applications, where yield strength describes the boundary of irreversible plastic deformation and toughness reflects the tolerance of fracture. We have investigated the tensile mechanical behaviors of the copper nanowires as well as the CNT/Cu nanocomposites under various mechanical loading conditions using molecular dynamics simulations. The size effect of copper nanowires has been examined. Two types of composites have been investigated where CNTs are either coated or embedded. We have studied the stress–strain relationship during the tensile loading process. We have obtained the Young's modulus, yield stress, toughness, and fracture strain of the composites, and compared them with the pristine copper nanowires. Furthermore, we have explored the effects of the temperatures and strain rates on the reinforcement.

2. Materials and methods

The MD simulations are used to model the tensile process of CNT/Cu composites. The MD simulations are implemented in the large-scale atomic/molecular massively parallel simulator (LAMMPS) software [38–40]. We have studied two configurations of composites as well as pristine copper nanowires. The simulation cells and atomic configurations in tensile test are shown in figure 1. For the CNT/Cu composites, we considered two configurations, namely *coated* and *embedded*, referring to that the CNTs are coated and embedded in copper, respectively. For the former, the CNTs

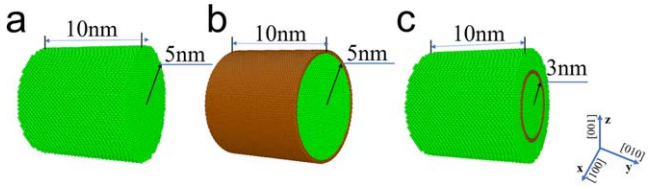

Figure 1. Simulation cell and atomic configurations of (a) pristine copper nanowire; (b) CNT/Cu nanocomposite with coated CNT; (c) CNT/Cu nanocomposite with embedded CNT.

are coated on the surface of the FCC copper nanowire, which has a length of 10 nm and a radius of 5 nm, shown in figure 1(b). The lattice constant of the copper nanowire is 3.615 Å. Figure 1(c) shows the embedded CNT/Cu composite, where the CNT with a radius of 3 nm is embedded into the copper nanowire. The periodic boundary condition is applied to the y direction while the x and z directions are fixed.

The potential function used in the MD simulations determined the accuracy of the results. The adaptive intermolecular reactive empirical bond order (AIREBO) potential has been widely used in carbon-based material simulations [41–44]. However, the original AIREBO potential is not suitable for fracture behaviors at large strains [45–50]. To avoid unphysical strain-hardening before fracture, the first-cutoff of C–C interaction ($r_{cc}^{\min}$) need to revise [51]. After extensive examination, we adopted $r_{cc}^{\min} = 1.92$ Å. However, we still have used the original version of $r_{cc}^{\min} = 1.70$ Å for reference. We denote these two potentials as *AR170* and *AR192* in this work for convenience. The well-known embedded-atom method (EAM) potential was used to describe the interatomic forces of the copper atoms [52, 53]. On account of that there was no C–Cu bond produced, therefore, only van der Waals forces exited between CNT and copper nanowire. We used the classical Lennard Jones (LJ) potential to parameterize the interactions between C and Cu atoms. Considering the different spatial distribution and stress state of the coated and embedded CNTs, we adopted different equilibrium interatomic distances σ and energy minimums ε for the coated and embedded nanocomposite cases. The LJ parameters σ and ε we adopted for the C–Cu interaction of the CNT/Cu nanocomposite with coated CNT are 3.0 Å and 0.0117 eV [54]. The corresponding parameters for the embedded nanocomposites are 2.84 Å and 0.0351 eV [36]. A cutoff distance of 3σ was chosen for the LJ potential function.

The copper and carbon atoms are created in the simulation box according to the appointed crystal lattices. The initial space between the CNT and inner/outer surface of the nanowire is less than 1 Å. To eliminate the initial abnormal stresses and stabilize the nano structures, an equilibration process was performed with 100 000 timesteps in both pristine copper nanowires and CNT/Cu nanocomposites. During the equilibration process, the space will be adjusted automatically by the Van der Waals' force (LJ potential), and infinitely approach the real-world situation finally. The context of NPT canonical ensemble was applied in the equilibration processes to control the positions and velocities of

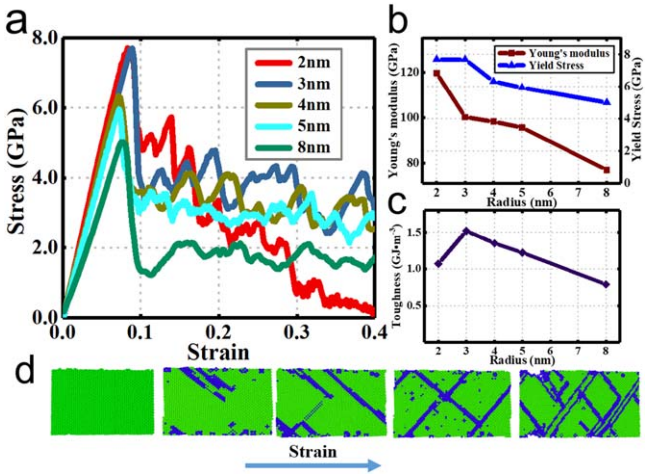

Figure 2. (a) Stress–strain curves, (b) Young's modulus, and (c) toughness of copper nanowires with varied radii from 2 to 8 nm; (d) dislocations evolutions during the tensile loading of the copper nanowire with the radius of 5 nm, corresponding to the strains of 0, 0.1, 0.2, 0.3, 0.4.

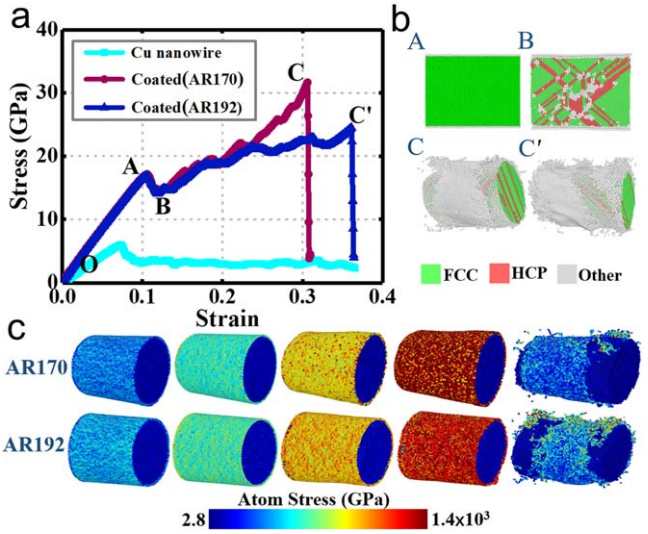

Figure 3. (a) Stress–strain curves of the two coated CNT/Cu nanocomposites and pristine copper nanowires; (b) snapshots of atomic structures at point A, B, C and C′; (c) the evolutions of local atomistic stresses during tensile loading process using AR170 potential (upper row) and AR192 potential (lower row). The corresponding strains of the first four snapshots are 0, 0.1, 0.2, 0.3. The last snapshot is after failure at strain of 0.306 and 0.361 for potential AR170 and AR192, respectively.

atoms. The Nose–Hoover algorithm was used to keep the temperature at 300 K in both equilibration and tensile loading [55, 56].

In the process of the tensile loading, a strain rate of $1 \times 10^9\ s^{-1}$ was imposed to the copper nanowire and CNT/Cu nanocomposites along the y direction (along the axis) within a context of NVT canonical ensemble. A timestep of 0.001 ps was adopted in all simulations.

3. Results and discussion

3.1. Tensile behaviors of copper nanowire with different radii

Firstly, we have explored the tensile behaviors of pristine copper nanowire with different radii for references to composites. The stress–strain curves have three stages: an elastic stage, a plastic stage, and a fracture stage during the tensile loading as shown in figure 2(a). In the initial elastic stage, the stress has a large growth rate with the increase of the strain till a peak value. The following abrupt stress drop indicates that the copper nanowires begin to undergo plastic deformation. In the plastic stage, stress fluctuates wildly and continually decreases until fracture.

The initial linear portion of the stress–strain curve is the linear elastic stage. The slope of the line is the Young's modulus [57]. Figure 2(b) shows the Young's modulus and yield stress of the copper nanowires. The Young's modulus of the copper nanowire with a radius of 5 nm is 95.6 GPa, consistent well with the experimental value of 90–110 GPa [57, 58], as well as a previous MD result of 95 GPa [59]. The yield stress of the copper nanowires is 7.7 GPa, consistent with the result of 7.32 GPa [60]. but lower than that of previous studies of about 12 GPa [36, 59]. The discrepancy in the yield stress is mainly ascribed to the interatomic potentials. Nevertheless, a general trend is that both the Young's modulus and yield stress decrease with the increase of the radius of the copper wire, which agrees well with the previous research on copper nanowire stretch [59]. Toughness is determined by integrating the stress–strain curves [61], which is described by $U_T = \int_0^{\epsilon_f} \sigma d\epsilon$, where ϵ_f is the fracture strain (a strain upon failure), and σ is the tensile stress. Figure 2(c) shows the toughness of the pristine copper nanowires. The toughness of the copper nanowire with a radius of 5 nm is 1.22 GJ m^{-3}, which shows a good agreement with previous studies [62–64]. It is reported that the size-dependent elasticity of the nanowires is attributed to the nonlinear effect of the nanowire core [65]. With the decrease of radius of the copper nanowire, the fraction of the surface atoms increases nonlinearly, resulting the increasing of the Young's modulus, yield stress, as well as the toughness. Figure 2(d) shows the dislocations produced in the tensile loading of the copper nanowire with a radius of 5 nm at 300 K. The strain rate is $1 \times 10^9\ s^{-1}$. The corresponding strains are 0, 0.1, 0.2, 0.3 and 0.4. The movie of the whole process is in supplementary information movie S1 available online at stacks.iop.org/NANO/31/115703/mmedia. We could see that the dislocations gradually fill the entire region inside the copper nanowire as the strain increases.

3.2. Tensile behaviors of CNT/Cu nanocomposites

The stress–strain curves of the coated CNT/Cu nanocomposite with different C–C interaction cutoffs and pristine copper nanowire with the same radius of 5 nm are shown in figure 3(a). The elastic deformation in the tensile loading of the coated composites can be divided into two stages: the OA and AC (AC′) stage. At the initial OA stage, both the CNT and the copper matrix have an elastic deformation, where the

Table 1. Young's modulus, strain, stress and toughness of Cu nanowires, coated and embedded CNT/Cu composites.

	Young's modulus (GPa)	Yield strain	Fracture strain		Yield stress (GPa)	Fracture stress (GPa)		Toughness (GJ m^{-3})	
			AR170	AR192		AR170	AR192	AR170	AR192
Cu nanowire(5 nm)	95.6		0.073			5.94		1.22	
CNT/Cu coated	161.3	0.106	0.306	0.361	17.1	31.7	24.5	5.46	6.17
CNT/Cu embedded	147.2	0.097	0.309	0.327	11.2	18.4	15.3	3.75	3.88

stress increases rapidly and is almost proportional to the strain. Then the copper matrix begins the plastic deformation while the CNT still has an elastic stretch, which is the AC (AC′) stage. In the AR170 study, the decrease of the stress produced in the copper matrix at the AC stage has a significant effect on the stress–strain curve trend due to the irregular elastic deformation. The CNT fractures at the point C (CNT yield), where the stress has a steep descent, indicating the failure of the materials. While in AR192 study, the increasing rate of the stress at AC′ stage is much lower than that of AR170 study on account of the lager $r_{cc}^{\min}$ of the C–C interaction. Meanwhile, the fracture strain is obviously larger than that in AR170 study.

The atomic configurations of the coated CNT/Cu nanocomposites at point A, B, C and C′ are displayed in figure 3(b). Many dislocations appear at point B (copper matrix yield) under the forced tension in the two coated nanocomposites, demonstrating the plastic deformation status of the copper matrix nanowire. The atom stress change during the tensile loading are figure 3(c). The stress on the CNT is much higher than that on the copper matrix, indicating the strong resistance of the CNTs during the tensile loading. Furthermore, when the strains approach fracture strain, the atom stress of the AR170 study is apparently higher than that of AR192 study, consistent with the stress–strain curves.

The Young's modulus calculated from the stress–strain curve of the coated CNT/Cu nanocomposite is 161.3 GPa (table 1), an increase of 68.7%, compared with the pristine copper nanowires. The yield stress of the coated CNT/Cu nanocomposites at point A is 17.1 GPa, with an increase of 187.9%, compared with the pristine copper nanowires. The fracture stress is 31.7 GPa and 24.5 GPa for AR170 and AR192 study, corresponding to an increase of 434% and 313%, respectively, referring to the pristine copper nanowire. Additionally, the yield strain of the nanocomposite is larger than that of the pristine copper nanowire, indicating that the coated CNT could effectively improve the ductility of the copper matrix. The toughness is 5.46 GJ m^{-3} and 6.17 GJ m^{-3} and for AR170 and AR192 study, respectively, which is corresponding to an increase of 347.5% and 405.7%, respectively, referring to the pristine copper nanowire. Such super reinforcement of the toughness implies broad applications of the CNT/Cu nanowires. The movie of the whole process is in the supplementary information movie S2 and S3 for AR170 and AR192 potential, respectively.

The stress–strain curves of the embedded CNT/Cu nanocomposites and pristine copper nanowires are shown in figure 4(a). Similar to the coated situation, there are also two stages, OA and AC (AC′) in the elastic deformation loading of the embedded nanocomposites. The stress–strain curves of the embedded composites with different C–C interaction cutoffs almost overlap, except the relatively lower fracture stress of AR192 study at point C′. The atomic structures at points A, B, C and C′ are shown in figure 4(b). It is found that the dislocations are mainly concentrated in the region inside the CNT at point B, which is due to the hindrance to the dislocation propagation by the CNTs. With the increasing of the tensile loading, the CNT breaks suddenly at points C and C′ of the embedded nanocomposites, then the CNT/Cu nanocomposite has failed. The atom stress of the embedded nanocomposites during the tensile loading is shown in figure 4(c). The local stress is centered around the CNT after the initial system equilibration process. Furthermore, the stress growth rate of the CNT is much faster than that of the copper matrix during the tensile loading, indicating the great contribution of the CNT on the high fracture strength of the CNT/Cu nanocomposite. The movie of the whole process is in the supplementary information movie S4 and S5 for AR170 and AR192 potential, respectively.

The parameters of the embedded CNT/Cu nanocomposites are also listed in table 1. The Young's modulus of the embedded nanocomposites is 147.2 GPa, very close to other simulation result of 145 GPa [36], with an increase of 54.0%, compared with the 95.6 GPa of the pristine copper nanowire. The yield stress at point A is 11.2 GPa, an increase of 88.6%, compared with the 5.94 GPa of the pristine copper nanowire. The fracture stress of the two embedded nanocomposites at points C and C′ are 18.4 GPa and 15.3 GPa, corresponding to the increases of 209.8% and 157.6%, respectively, compared with the pristine copper nanowire. The toughness is 3.75 GJ m^{-3} and 3.88 GJ m^{-3} and for AR170 and AR192 study in embedded ones, corresponding to an increase of 207.4% and 218.0%, respectively, referring to the pristine copper nanowires.

In general, both the coated and embedded composites have a significant reinforcement on mechanical properties. Meanwhile, the coated composites possess larger Young's modulus, yield stress and toughness than that of embedded ones. Further analysis shows that the local stress produced around the embedded CNT reduces the Young's modulus and

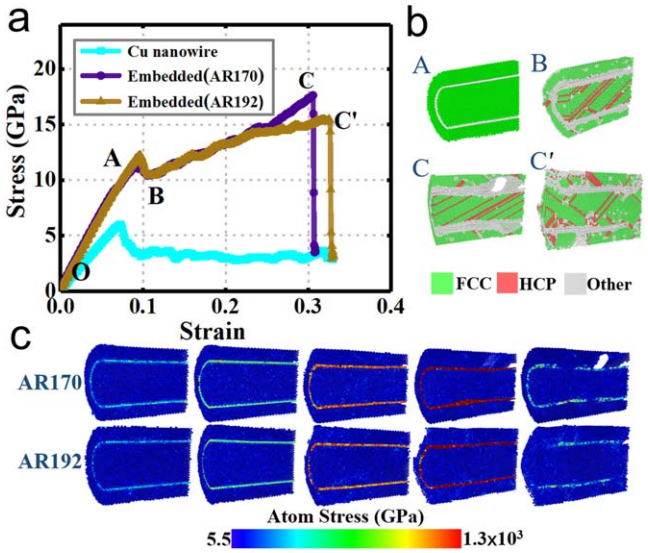

Figure 4. (a) Stress–strain curves of the embedded CNT/Cu nanocomposites and pristine copper nanowires; (b) snapshots of atomic structures at point A, B, C and C′; (c) the evolutions of local atomistic stresses during tensile loading process using AR170 potential (upper row) and AR192 potential (lower row). The corresponding strains of the first four snapshots are 0, 0.1, 0.2, 0.3. The last snapshot is after failure at strain of 0.306 and 0.327 for potential AR170 and AR192, respectively.

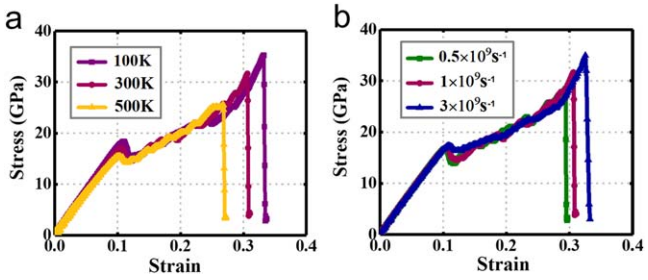

Figure 5. Stress–strain curves of the coated CNT/Cu nanocomposites in (a) different temperatures and (b) different strain rates.

yield stress by hindering the dislocation motion and weakening the deformation bearing capacity. It is worth noting that in the coated composite case, the CNT has a very slight effect on the dislocation propagation. In the embedded composite case, the embedded CNT has a significant hindrance on the dislocation extending and propagation, as shown in figure 4(b). Due to the boundary confinement, their effects on the nucleation of dislocation are similar.

3.3. Temperature effect

To investigate the finite temperature effect on mechanical behaviors, we have carried out the tensile simulations of the coated nanocomposites using $r_{cc}^{\min} = 1.7$ Å at three different temperatures: 100, 300, and 500 K. The results of the stress–strain curves are shown in figure 5(a). The tensile behaviors are sensitive to the environment temperatures. The higher temperature significantly reduce the max yield stress and strain by softening the crystalline structure and decreasing the grain boundary strength [66, 67], which weakens the loading bearing capacity of the CNT and copper matrix. The Young's modulus and toughness also have a reduction with the decrease in the whole strength and stiffness of the CNT nanocomposite.

3.4. Effect of strain rate

We have carried out the tensile simulations of the coated nanocomposites using $r_{cc}^{\min} = 1.7$ Å at three different loading rates. The tensile stress–strain curves are displayed in figure 5(b). The three yield stresses are similar. The three Young's modulus are the same for three strain rates. Our results indicate that the yield stresses are insensitive to the strain rate. However, there are considerable difference in the fracture stress. It is indicated that the CNTs have a better malleability during deformation with a higher strain rate. As the strain rate get lower, the thermal fluctuations get longer and are more likely to overcome the energy barrier of the C–C bonds, resulting in the reduction of the ultimate tensile strain and stress. The linear mechanical properties of the copper matrix are almost impervious to the change of the tensile strain rate, opposed to that of nonlinear mechanics including fracture strength and toughness. It is worth noting that the strain rates in our MD simulations are much higher than any real experiments due to the limitations of MD methods. Further studies with low strain rates are interesting, but they are outside the scope of feasible molecular dynamics simulations.

Our MD results present the enhancement on the copper nanowire matrix by the CNT, which is in line with previous studies on CNT-reinforced nanocomposites [68–70]. In our tensile simulations, the nanocomposite with coated CNT has the strongest reinforcement with a Young's modulus of 161.3 GPa and the fracture strength of 31.7 GPa, corresponding to the increases of 68.7% and 433.7%, compared with the pristine copper nanowire. The toughness is 6.17 GJ m^{-3}, about 5.1 times of that of pristine copper nanowire.

4. Conclusions

We have systematically investigated the tensile characteristics of CNT enhanced copper nanowires by means of molecular dynamics simulations. We have examined two configurations of CNT/Cu nanocomposites, coated and embedded, with different sizes, loading rates, and temperatures. The double peaks in the stress–strain curves implies distinct ductility of the CNT/Cu nanocomposite. Both the coated and embedded CNTs have an enhancement on the Young's modulus, yield stress, and toughness owing to the excellent loading bearing capacity of the CNT. Meanwhile, the coated nanocomposites have the stronger reinforcement than the embedded ones on account of more local stress produced in the embedded situations. A reinforcement of over fivefold in both yield strength (5.3 times) and toughness (5.1 times) has been achieved when the carbon nanotubes are coated on the copper nanowires, in addition to 1.7 times in the Young's modulus. Additionally, it is demonstrated that high temperature can

significantly reduce the whole strength and stiffness of the CNT/Cu nanocomposite by weakening the lattice intensity. The CNT/Cu nanocomposites have a higher yield stress when the strain rate is larger. Our studies provide insights in optimizing mechanical properties of CNT/Cu nanocomposites, which might be useful in material design for modern integrated circuits and semiconductor technology.

Acknowledgments

We acknowledge the generous financial support from by the National Natural Science Foundation of China (No. 51727901). The numerical calculations in this paper were conducted on the supercomputing system at the Supercomputing Center of Wuhan University.

Author contributions

PW, QC and QP conceived the idea and wrote the paper. PW, HW and YN did the simulations. PW and SL performed the data analysis. All the authors had full discussions and comments on the paper.

Additional information

There are five movies in the supplementary information showing the tensile processes for pristine copper nanowires, coated and embedded CNT/Cu composite nanowires.

Conflicts of interest

The authors declare no conflict of interest.

Data availability

All data generated or analyzed during this study are included in this published article and its supplementary information files.

ORCID iDs

Qiang Cao https://orcid.org/0000-0003-0696-0523

References

[1] Iijima S 1991 Helical microtubules of graphitic carbon *Nature* **354** 56–8
[2] Baughman RH, Zakhidov AA and de Heer WA 2002 Carbon nanotubes-the route toward applications *Science* **297** 787–92
[3] Holt JK, Park HG, Wang YM, Stadermann M, Artyukhin AB, Grigoropoulos CP, Noy A and Bakajin O 2006 Fast mass transport through sub-2-nanometer carbon nanotubes *Science* **312** 1034–7
[4] Majumder M, Chopra N, Andrews R and Hinds BJ 2005 Nanoscale hydrodynamics: enhanced flow in carbon nanotubes *Nature* **438** 44
[5] Sun DM, Timmermans MY, Tian Y, Nasibulin AG, Kauppinen EI, Kishimoto S, Mizutani T and Ohno Y 2011 Flexible high-performance carbon nanotube integrated circuits *Nat. Nanotechnol.* **6** 156–61
[6] Shi JD *et al* 2019 Smart textile-integrated microelectronic systems for wearable applications *Adv. Mater.* 1901958
[7] Yan W, Page A, Tung ND, Qu YP, Sordo F, Wei L and Sorin F 2019 Advanced multimaterial electronic and optoelectronic fibers and textiles *Adv. Mater.* **31** 1802348
[8] Weng W, Yang JJ, Zhang Y, Li YX, Yang S Y, Zhu L P and Zhu M F 2019 A route toward smart system integration: from fiber design to device construction *Adv. Mater.* 1902301
[9] Loos M R and Schulte K 2011 Is it worth the effort to reinforce polymers with carbon nanotubes? *Macromol. Theory Simul.* **20** 350–62
[10] Loos M R and Manas-Zloczower I 2012 Reinforcement efficiency of carbon nanotubes—myth and reality *Macromol. Theory Simul.* **21** 130–7
[11] Zhou C, Wang S, Zhuang Q and Han Z 2008 Enhanced conductivity in polybenzoxazoles doped with carboxylated multi-walled carbon nanotubes *Carbon* **46** 1232–40
[12] Veedu V P, Cao A Y, Li X S, Ma K G, Soldano C, Kar S, Ajayan P M and Ghasemi-Nejhad M N 2006 Multifunctional composites using reinforced laminae with carbon-nanotube forests *Nat. Mater.* **5** 457–62
[13] Bakshi S R, Lahiri D and Agarwal A 2010 Carbon nanotube reinforced metal matrix composites-a review *Int. Mater. Rev.* **55** 41–64
[14] Salvetat J P, Bonard J M, Thomson N H, Kulik A J, Forro L, Benoit W and Zuppiroli L 1999 Mechanical properties of carbon nanotubes *Appl. Phys.* A **69** 255–60
[15] Neubauer E, Kitzmantel M, Hulman M and Angerer P 2010 Potential and challenges of metal-matrix-composites reinforced with carbon nanofibers and carbon nanotubes *Compos. Sci. Technol.* **70** 2228–36
[16] Munir K S, Kingshott P and Wen C 2015 Carbon nanotube reinforced titanium metal matrix composites prepared by powder metallurgy—a review *Crit. Rev. Solid State* **40** 38–55
[17] Chen W X, Tu J P, Wang L Y, Gan H Y, Xu Z D and Zhang X B 2003 Tribological application of carbon nanotubes in a metal-based composite coating and composites *Carbon* **41** 215–22
[18] Inoue S and Matsumura Y 2008 Molecular dynamics simulation of metal coating on single-walled carbon nanotube *Chem. Phys. Lett.* **464** 160–5
[19] Inoue S and Matsumura Y 2009 Influence of metal coating on single-walled carbon nanotube: molecular dynamics approach to determine tensile strength *Chem. Phys. Lett.* **469** 125–9
[20] Ji D K, Yun H, Kim G C, Lee C W and Choi H C 2013 Antibacterial activity and reusability of CNT-Ag and GO-Ag nanocomposites *Appl. Surf. Sci.* **283** 227–33
[21] Feng Y, Xiao W, Daqi Z, Juan Y, Da L, Ziwei X, Jiake W, Jian-Qiang W, Zhi X and Fei P 2014 Chirality-specific growth of single-walled carbon nanotubes on solid alloy catalysts *Nature* **510** 522–4
[22] Moghadam A D, Omrani E, Menezes P L and Rohatgi P K 2015 Mechanical and tribological properties of self-lubricating metal matrix nanocomposites reinforced by carbon nanotubes (CNTs) and graphene-a review *Composites* B **77** 402–20

[23] Esawi A M K, Morsi K, Sayed A, Tahera M and Lanka S 2010 Effect of carbon nanotube (CNT) content on the mechanical properties of CNT-reinforced aluminium composites *Compos. Sci. Technol.* **70** 2237–41

[24] Perez-Bustamante R, Estrada-Guel I, Antunez-Flores W, Miki-Yoshida M, Ferreira P J and Martinez-Sanchez R 2008 Novel Al-matrix nanocomposites reinforced with multi-walled carbon nanotubes *J. Alloy Compd.* **450** 323–6

[25] Bakshi S R, Singh V, Balani K, McCartney D G, Seal S and Agarwal A 2008 Carbon nanotube reinforced aluminum composite coating via cold spraying *Surf. Coat. Technol.* **202** 5162–9

[26] Liu S Z, Xie L, Peng Q and Li R 2019 Carbon nanotubes enhance the radiation resistance of bcc iron revealed by atomistic study *Materials* **12** 217

[27] Choi B K, Yoon G H and Lee S 2016 Molecular dynamics studies of CNT-reinforced aluminum composites under uniaxial tensile loading *Composites* B **91** 119–25

[28] Liu H, Xun S, Xu F, Zhang L, Zhang W, Chen L, Qiang L, Uher C, Day T and Snyder G J 2012 Copper ion liquid-like thermoelectrics *Nat. Mater.* **11** 422–5

[29] Kiener D, Hosemann P, Maloy S A and Minor A M 2011 *In situ* nanocompression testing of irradiated copper *Nat. Mater.* **10** 608–13

[30] Guermoune A, Chari T, Popescu F, Sabri S S, Guillemette J, Skulason H S, Szkopek T and Siaj M 2011 Chemical vapor deposition synthesis of graphene on copper with methanol, ethanol, and propanol precursors *Carbon* **49** 4204–10

[31] Huang J, Chen M, Chen H, Chen S and Sun Q 2014 Leaching behavior of copper from waste printed circuit boards with Brønsted acidic ionic liquid *Waste Manage.* **34** 483–8

[32] Sun F W and Li H 2011 Torsional strain energy evolution of carbon nanotubes and their stability with encapsulated helical copper nanowires *Carbon* **49** 1408–15

[33] Zheng Y G, Sun J, Ye H F, Zhang J Y and Zhang H W 2018 Crystallization behaviors and mechanical properties of carbon nanotube encapsulated copper nanowires *Comput. Mater. Sci.* **143** 350–9

[34] Duan K, Li L, Hu Y J and Wang X L 2017 Enhanced interfacial strength of carbon nanotube/copper nanocomposites via Ni-coating: Molecular-dynamics insights *Physica* E **88** 259–64

[35] Duan K, Li L, Hu Y J and Wang X L 2017 Damping characteristic of Ni-coated carbon nanotube/copper composite *Mater. Des.* **133** 455–63

[36] Faria B, Guarda C, Silvestre N, Lopes J N C and Galhofo D 2018 Strength and failure mechanisms of cnt-reinforced copper nanocomposite *Composites* B **145** 108–20

[37] 1941 Skin effect in composite and ferromagnetic wires *Nature* **147** 719

[38] Wang P, Cao Q, Yan Y, Nie Y, Liu S and Peng Q 2019 Graphene surface reinforcement of iron *Nanomaterials* **9** 59

[39] Wang H, Cao Q, Peng Q and Liu S 2019 Atomistic study of mechanical behaviors of carbon honeycombs *Nanomaterials* **9** 109

[40] Peng Q, Meng F J, Yang Y Z, Lu C Y, Deng H Q, Wang L M, De S and Gao F 2018 Shockwave generates ⟨100⟩ dislocation loops in bcc iron *Nat. Commun.* **9** 4880

[41] Stuart S J, Tutein A B and Harrison J A 2000 A reactive potential for hydrocarbons with intermolecular interactions *J. Chem. Phys.* **112** 6472–86

[42] Dewapriya M A N and Meguid S A 2017 Atomistic modeling of out-of-plane deformation of a propagating Griffith crack in graphene *Acta Mech.* **228** 3063–75

[43] Zheng S, Cao Q, Liu S and Peng Q 2018 Atomic structure and mechanical properties of twisted bilayer graphene *J. Compos. Sci.* **3** 2

[44] Wang L, Jin J F, Cao J Y, Yang P J and Peng Q 2018 Interaction of edge dislocations with graphene nanosheets in graphene/Fe composites *Crystals* **8** 160

[45] Deng B, Jie H, Zhu H, Sheng L, Liu E, Shi Y and Peng Q 2017 The normal-auxeticity mechanical phase transition in graphene *2D Mater.* **4** 021020

[46] Jeong B W, Lim J K and Sinnott S B 2007 Tensile mechanical behavior of hollow and filled carbon nanotubes under tension or combined tension-torsion *Appl. Phys. Lett.* **90** 622

[47] Grantab R, Shenoy V B and Ruoff R S 2010 Anomalous strength characteristics of tilt grain boundaries in graphene *Science* **330** 946–8

[48] Li R, Wang S and Peng Q 2018 Tuning the slide-roll motion mode of carbon nanotubes via hydroxyl groups *Nanoscale Res. Lett.* **13** 138

[49] Sammalkorpi M, Krasheninnikov A, Kuronen A, Nordlund K and Kaski K 2004 Mechanical properties of carbon nanotubes with vacancies and related defects *Phys. Rev.* B **70** 121–7

[50] Wei Y J, Wu J T, Yin H Q, Shi X H, Yang R G and Dresselhaus M 2012 The nature of strength enhancement and weakening by pentagon-heptagon defects in graphene *Nat. Mater.* **11** 759–63

[51] Hou J, Deng B, Zhu H X, Lan Y, Shi Y, De S, Liu L, Chakraborty P, Gao F and Peng Q 2019 Magic auxeticity angle of graphene *Carbon* **149** 350–4

[52] Zhou X W *et al* 2001 Atomic scale structure of sputtered metal multilayers *Acta Mater.* **49** 4005–15

[53] Xie L, An H, Peng Q, Qin Q and Zhang Y 2018 Sensitive five-fold local symmetry to kinetic energy of depositing atoms in Cu–Zr thin film growth *Materials* **11** 2548

[54] Wang W H, Peng Q, Dai Y Q, Qian Z F and Liu S 2016 Distinctive nanofriction of graphene coated copper foil *Comput. Mater. Sci.* **117** 406–11

[55] Hoover W G 1985 Canonical dynamics-equilibrium phase-space distributions *Phys. Rev.* A **31** 1695–7

[56] Nose S 1984 A unified formulation of the constant temperature molecular-dynamics methods *J. Chem. Phys.* **81** 511–9

[57] Sanders P G, Eastman J A and Weertman J R 1996 Tensile behavior of nanocrystalline copper *Process. Prop. Nanocryst. Mater.* 379–86

[58] Staller O, Mitterbauer C and Mayr K 2008 Tensile strengths and Young's modulus of thin copper and copper-nickel (CuNi44) substrates *Cent. Eur. J. Chem.* **6** 535–41

[59] Rohith P, Sainath G and Choudhary B K 2017 Molecular dynamics simulation studies on the influence of aspect ratio on tensile deformation and failure behaviour of (1 0 0) copper nanowires *Comput. Mater. Sci.* **138** 34–41

[60] Peng Q, Zhang X and Lu G 2009 Structure, mechanical and thermodynamic stability of vacancy clusters in Cu *Modelling. Simul. Mater. Sci. Eng.* **18** 55009–25

[61] Ritchie R O 2011 The conflicts between strength and toughness *Nat. Mater.* **10** 817–22

[62] Shabib I and Miller R E 2009 A molecular dynamics study of twin width, grain size and temperature effects on the toughness of 2D-columnar nanotwinned copper *Modelling Simul. Mater. Sci. Eng.* **17** 055009

[63] Roman R E and Cranford S W 2014 Strength and toughness of graphdiyne/copper nanocomposites *Adv. Eng. Mater.* **16** 862–71

[64] Mohammadi B, Tavoli M and Djavanroodi F 2014 Effects of constrained groove pressing (CGP) on the plane stress fracture toughness of pure copper *Struct. Eng. Mech.* **52** 957–69

[65] Liang H Y, Upmanyu M and Huang H C 2005 Size-dependent elasticity of nanowires: nonlinear effects *Phys. Rev.* B **71** 241403

[66] Jeong W and Kessler M R 2009 Effect of functionalized MWCNTs on the thermo-mechanical properties of poly(5-

ethylidene-2-norbornene) composites produced by ring-opening metathesis polymerization *Carbon* **47** 2406–12
[67] Zhang Y Y and Gu Y T 2013 Mechanical properties of graphene: effects of layer number, temperature and isotope *Comput. Mater. Sci.* **71** 197–200
[68] Guo S H, Zhu B E, Ou X D, Pan Z Y and Wang Y X 2010 Deformation of gold-filled single-walled carbon nanotubes under axial compression *Carbon* **48** 4129–35
[69] Silvestre N, Faria B and Lopes J N C 2014 Compressive behavior of CNT-reinforced aluminum composites using molecular dynamics *Compos. Sci. Technol.* **90** 16–24
[70] Coleman J N, Khan U, Blau W J and Gun'Ko Y K 2006 Small but strong: a review of the mechanical properties of carbon nanotube–polymer composites *Carbon* **44** 1624–52